Optical trapping and transport of ultracold erbium atoms

Péter Juhász

Pembroke College

University of Oxford

A report submitted to transfer to the status of

Doctor of Philosophy

Trinity 2019

Abstract

Many ultracold atoms experiments use two linked vacuum chambers, so it is necessary to transport atomic clouds over several tens of cm. This report describes the design, construction and testing of a proposed all-optical system for trapping and transporting ultracold erbium atoms. The system uses a high-power laser beam to create an optical dipole trap for the atoms, and lenses whose focal length can be tuned electronically to change the trap position. The theory of the proposed system is reviewed and the project is put into the context of the wider experiment. Results of tests of the transport system are presented and the building of the test version of the transport system is reported.

Contents

1 Introduction

1.1 Overview of ultracold atom systems

Ultracold atoms are used widely to test several aspects of quantum theory. Being able to produce quantum condensates opened the possibility of a range of experiments, with applications ranging from atom interferometry [1], precision measurements [2] and atomtronics [3] to quantum simulation [4].

Traditionally, ultracold atomic gases are confined in harmonic trapping potentials, realised by Gaussian laser beams or magnetic traps. However, this does not reflect the continuous translational symmetry that many systems possess. This problem was overcome by placing the atoms in a so-called optical box potential [5], which cleared the way for many interesting topics to be examined, including the dynamics of passing through a phase transition at a finite rate [6], weak collapse in a Bose–Einstein Condensate (BEC) [7] and turbulence in a quantum gas [8].

Recent developments in laser cooling expanded the spectrum of elements that can be condensed, including some with very high magnetic moments [9–11]. This adds a new dimension to experiments that can be realized, introducing long-range and anisotropic, dipole-dipole interactions (DDI) on top of the short-range and isotropic contact interactions present in all atomic species [12]. Using these dipolar quantum gases, there are considerable efforts [13–18] to create a supersolid, a counter-intuitive state of matter that combines the dissipationless flow of a superfluid with the crystal-like periodic density modulation of a solid [19]. It was proposed that this density modulation could be achieved via the self-organisation of an excited dipolar quantum gas into quantum droplets [20–22], caused by their special ('roton-like') excitation spectrum [23–25].

1.2 Overview of this experiment

The aim of our experiment is to create a dipolar erbium BEC in a 2D pancake-like uniform trapping potential. The homogeneity of the trapping potential is crucial for accessing the full flavour of the physics that stems from the long-range nature of the interatomic forces. Once the core of the experimental setup is completed, we plan to first carry out a few technical measurements, measuring the polarisability and scattering rates [26]. Once these are completed, we aim to explore phenomena expected to occur in dipolar quantum gases, starting from roton physics [24], measuring the roton spectrum [27] and how long-range interactions affect the critical velocity [28, 29] and the critical temperature [30]. Furthermore, we plan to explore the influence of long-range interactions on out-of-equilibrium physics. Specifically, we are interested in scenarios that have already been attractive subjects in the field, including driven [8] and quenched [6] systems. Finally, the long-term project plan is to add a second atomic species, potassium, to expand the range of phenomena we can explore. These will include polaron physics [31, 32] and subjects relevant to quantum information, like qubit decoherence control [33, 34].

An overview of the apparatus can be seen in Fig. 1. Erbium is supplied via an effusion cell oven[1] emitting an atomic beam into our vacuum chamber. This beam first interacts with

[1] DFC-40-10-WK-2B-SHE, from Createc.

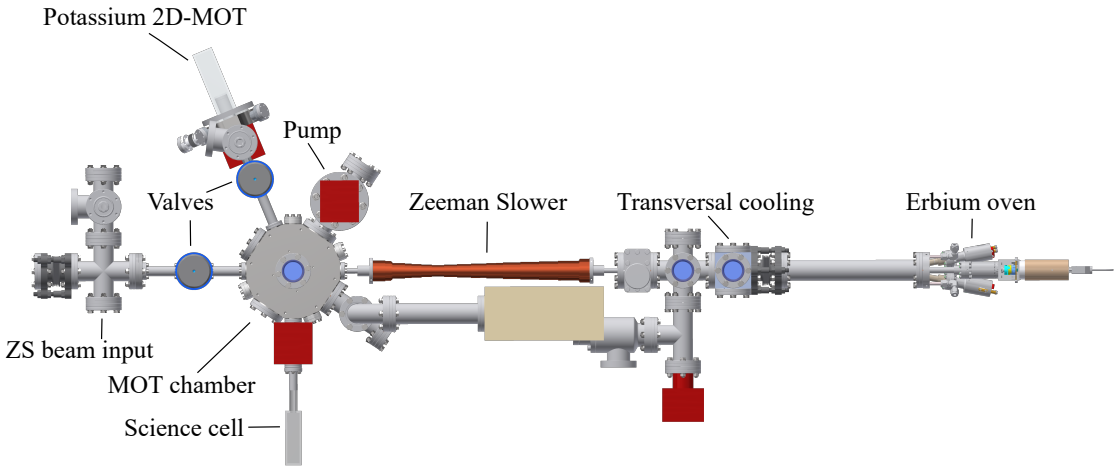

Figure 1. The vacuum chamber of the experiment. Atoms enter from the erbium oven and then encounter transversal cooling. They then propagate down the Zeeman slower where they are slowed down before being captured in the MOT chamber. Finally they are transferred to the science cell with enhanced optical access.

transversal cooling (TC) beams, which help collimate the beam by slowing it perpendicular to its propagation direction. After this, the beam enters the Zeeman slower (ZS), which consists of a counter-propagating laser beam and magnetic coils creating a spatially varying field that keeps the atoms on resonance, as they slow down, using the Zeeman effect [35]. These both use a broad atomic transition at 401 nm (blue) with a natural linewidth of 29.7 MHz, giving a Doppler temperature of 714 µK, meaning it is very convenient for the initial stages of cooling [36]. The Zeeman slower has a designed capture velocity of 465 m s^{-1} and slows the atoms down to 6 m s^{-1} [37].

As the atoms slow down they reach the central part of our vacuum chamber, where they are already slow enough to be trapped using a Magneto-Optical Trap [38] (MOT). The MOT operates on a transition at 583 nm (yellow) that has a natural linewidth of 190 kHz, giving a Doppler temperature of 4.6 µK. The MOT has a designed capture velocity of 7 m s^{-1} [37]. In practice, atoms should reach a final temperature of 10 µK and a density of 1.5×10^{11} cm^{-3} [39]. These atoms are cold enough to be directly loaded into an Optical Dipole Trap [40] (ODT) used for evaporative cooling.

In our experiment, two linked vacuum chambers are used, one for initial cooling and one for the final experiment, to allow optical access around the glass 'science cell'. Therefore, it is necessary to transport the atomic cloud over 50 cm. Sometimes this is done with overlapping magnetic coils [41] or by physically moving one coil pair [42, 43], but the state we use is not magnetically trappable. A different method is an all-optical transport which can be performed by displacing the focus of a dipole beam in which the atoms are trapped. This has been achieved with the focusing lens mounted on an air-bearing translation stage [44], but it comes with the drawback of placing a cumbersome system close to the vacuum chamber, which bears the risk of transferring vibrations to the dipole trap or the optical table.

An alternative all-optical approach was also demonstrated [45], which involves using

focus-tuneable lenses: lenses filled with a liquid that change their focal length in response to an applied current. Atoms are trapped in the focal point of the beam (the ODT), which is then moved from the MOT chamber to the science cell by tuning the focal length of the lenses (an optical tweezer). As this eliminates the risk of transferring vibrations we decided on this solution. This project focused on the design and building of this system.

Sec. 2 explains the theoretical background of optical trapping and transporting the atoms. The transport system is discussed in more detail in Sec. 3, focusing on system design and results from the test implementation. An outlook to future directions is presented in Sec. 4.

2 Theory

2.1 Optical Dipole Trap

Optical trapping of atoms is an important aspect of many ultracold atom experiments. A basic introduction into the theory of optical dipole traps is presented below, largely following previous work in this area [36, 40, 46, 47].

An intuitive model of the optical dipole trap can be devised by considering a neutral atom placed in an oscillating electric field. In this field $\mathbf{E}(\mathbf{r}, t)$ the centres of mass of the positive and negative charges are periodically separated by the field, which means that an oscillating electric dipole $\mathbf{p}(\mathbf{r}, t)$ is induced:

$$\mathbf{p}(\mathbf{r}, t) = \alpha \mathbf{E}(\mathbf{r}, t), \tag{1}$$

where α is the complex polarisability of the atom which in general has a tensorial character and depends on the atomic species, the light frequency, the polarisation of the electric field θ_p and the propagation direction θ_k with respect to the quantisation axis (the direction of the magnetic field B). The atom can then be treated as a dipole that interacts with the driving field. The dipole energy can be calculated as:

$$U_{\mathrm{dip}}(\mathbf{r}) = -\frac{1}{2} \langle \mathbf{p}(\mathbf{r}, t) \cdot \mathbf{E}(\mathbf{r}, t) \rangle = -\frac{1}{2\varepsilon_0 c} \mathrm{Re}(\alpha) I(\mathbf{r}), \tag{2}$$

where the relation for the field intensity $I(\mathbf{r}) = \frac{1}{2}\varepsilon_0 c |\mathbf{E}(\mathbf{r})|^2$ is used, ε_0 is the vacuum permittivity, c is the speed of light and $\mathbf{E}(\mathbf{r})$ is the field amplitude.

When the dipole is driven below resonance ('red-detuned' regime) it oscillates in phase with the field and when it is driven above resonance ('blue-detuned' regime) it oscillates out of phase. Below (above) resonance the interaction energy is negative (positive) and therefore the atom is attracted to (repelled from) the region with the highest electric field intensity. A trap will be created for negative interaction energies where the atoms are drawn to the focus of a Gaussian laser beam (where it has its highest intensity).

The driven oscillator also absorbs energy, which is then re-emitted as dipolar radiation. This can also be seen as a photon scattering process, where the photon is absorbed by the atom and then spontaneously re-emitted, each time leading to a momentum transfer, which can lead to heating and atoms being ejected from the trap. For a detuning δ from a given atomic transition the interaction energy is given by $U_{\mathrm{dip}} \propto I/\delta$, while the scattering rate is $\Gamma_{\mathrm{sc}} \propto I/\delta^2$, so scattering is suppressed for large detunings at the same trap depth [46].

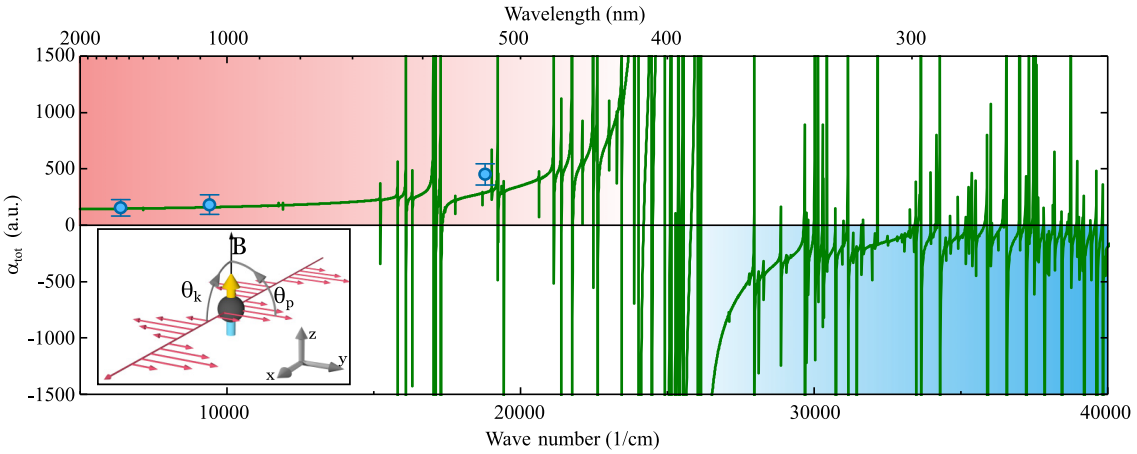

Figure 2. Atomic polarisability α of Er in the ground state for $\theta_p = \theta_k = 90°$ as a function of the light-field wavelength. A divergence of the polarisability indicates an optical dipole transition. The red and blue regions indicate the broad red-detuned region for long wavelengths and a blue-detuned region in the ultraviolet range. The inset illustrates the configuration of angles θ_k and θ_p for the shown data. B denotes the orientation of the magnetic field. We see there is a large range of wavelengths $\lambda > 700\,\text{nm}$ suitable for trapping. Illustration taken from [26].

To calculate the trap depth and trapping frequencies, we need to know the polarisability of erbium and the intensity distribution of the light. The polarisability was calculated and measured at different wavelengths [26, 48] and can be seen in Fig. 2. The intensity distribution of an elliptical Gaussian beam is

$$I(x,y,z) = \frac{2P}{\pi w_x(z) w_y(z)} e^{-2\left(\frac{x^2}{w_x^2(z)} + \frac{y^2}{w_y^2(z)}\right)}, \tag{3}$$

where P is the total power in the beam. For small atomic clouds compared to the size of the laser beam we can use a harmonic approximation of the dipole potential (Eq. (2)) to extract the trap frequencies. We see:

$$U_{\text{dip}} \approx \frac{1}{2}\frac{\partial^2 U_{\text{dip}}}{\partial x^2}\bigg|_0 + \frac{1}{2}\frac{\partial^2 U_{\text{dip}}}{\partial y^2}\bigg|_0 + \frac{1}{2}\frac{\partial^2 U_{\text{dip}}}{\partial z^2}\bigg|_0 \tag{4}$$

$$= -\frac{1}{2\varepsilon_0 c}\,\text{Re}(\alpha)\frac{2P}{\pi w_x w_y}\left(1 - \frac{2x^2}{w_x^2} - \frac{2y^2}{w_y^2} - \frac{1}{2}z^2\left(\frac{1}{z_{Rx}^2} + \frac{1}{z_{Ry}^2}\right)\right), \tag{5}$$

where w_x and w_y are the beam waists in the x and y direction, respectively, and z_{Rx} and z_{Ry} are the respective Rayleigh ranges. From here, we see the total trap depth is

$$U_0 = -\frac{1}{2\varepsilon_0 c}\,\text{Re}(\alpha)\frac{2P}{\pi w_x w_y}, \tag{6}$$

which is sometimes expressed as a temperature, $T_0 = U_0/k_B$, where k_B is the Boltzmann constant. By comparing the trapping potential (Eq. (5)) to the potential of a simple harmonic

oscillator ($\frac{1}{2}m(\omega_x^2x^2+\omega_y^2y^2+\omega_z^2z^2)$), the trapping frequencies can be extracted as

$$\omega_x = \sqrt{\frac{4U_0}{mw_x^2}} = \sqrt{\frac{4\alpha P}{m\varepsilon_0 c\pi w_x^3 w_y}}, \tag{7}$$

$$\omega_y = \sqrt{\frac{4U_0}{mw_y^2}} = \sqrt{\frac{4\alpha P}{m\varepsilon_0 c\pi w_x w_y^3}}, \tag{8}$$

$$\omega_z = \sqrt{\frac{2U_0}{mz_{R_{\text{eff}}}^2}} = \sqrt{\frac{\alpha P\lambda^2(w_x^4+w_y^4)}{m\varepsilon_0 c\pi^3 w_x^5 w_y^5}}, \tag{9}$$

where $z_{R_{\text{eff}}} = \frac{z_{Rx}z_{Ry}}{\sqrt{\frac{1}{2}(z_{Rx}^2+z_{Ry}^2)}} = \sqrt{\frac{2}{w_x^4+w_y^4}}\frac{w_x^2w_y^2\pi}{\lambda}$ is the effective Rayleigh range.

2.2 Time-averaged potentials

Further to changing the incoming beam size and power, the trap size and depth can also be changed by periodically moving (dithering) the trapping beam. If the beam is dithered at a much higher frequency than the trapping frequency, the atoms are not able to follow the motion of the light and instead experience an effective time-averaged potential. Creating an elongated trap is useful as a larger overlap with the MOT is then possible enabling a higher ODT loading efficiency.

If the beam's position is given by the periodic functions $x_D(t), y_D(t)$ with period T, the time-averaged potential is

$$U(x,y) = \frac{U_0}{T}\int_0^T e^{-\left(\frac{2(x_D(t)-x)^2}{w_x^2}+\frac{2(y_D(t)-y)^2}{w_y^2}\right)}\,\mathrm{d}t\,, \tag{10}$$

where U_0 is the original trap depth and $w_{x,y}$ are the original beam waists. We would like the effective potential to be the usual Gaussian, but elliptic in one direction (let this be x). Unfortunately, an analytic solution for $x_D(t)$ cannot be given, but if the dithering functions are the periodic functions

$$x_D(t) = \begin{cases} \frac{2A}{\pi}\arcsin\left(\frac{4t}{T}-1\right) & \text{if } 0 \le t \le \frac{T}{2}, \\ -\frac{2A}{\pi}\arcsin\left(\frac{4t}{T}-3\right) & \text{if } \frac{T}{2} \le t \le T, \end{cases} \tag{11}$$

$$y_D(t) = 0, \tag{12}$$

the resulting potential $U(x,y)$ is approximately Gaussian [49]. The approximation is best if the dithering amplitude A is not much bigger than the original beam waists w_x, w_y. A plot of the dithering function and the resulting potential can be seen in Fig. 3.

It was decided that an acousto-optic modulator[2] (AOM) will be used to dither the beam, which can also be used to control the laser power. An AOM works by creating a sound wave travelling through a crystal, which periodically alters the refractive index of the medium.

[2] AOMO 3110-197, from Gooch & Housego.

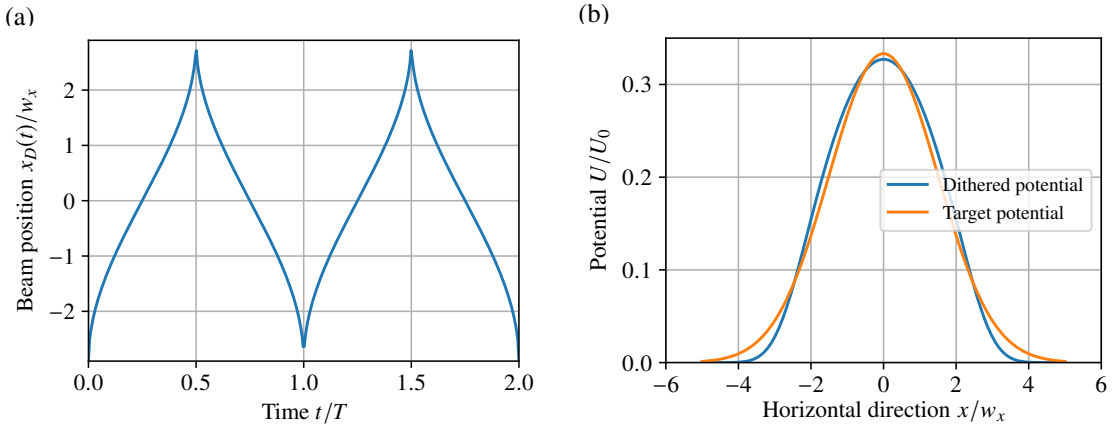

Figure 3. (a) Plot of the dithering function described in Eq. (11) with $A = 2.9w_x$. An arcsin function is used to generate a roughly Gaussian potential with increased waist. (b) The resulting potential (blue) compared with the best fit (target) Gaussian potential with waist $3w_x$ (orange). We see the dithered potential is close to Gaussian, but is not exactly the same.

This acts as a layered structure from which light can be reflected into Bragg peaks. The first order deflection angle of the AOM is governed by the Bragg condition

$$2\frac{v_s}{f_{\text{AOM}}}\sin(\theta_d) = \lambda, \tag{13}$$

where θ_d is the deflection angle, λ is the light wavelength, f_{AOM} is the driving frequency and v_s is the speed of sound. Therefore, changing the driving frequency of the AOM will affect the deflection angle and move the beam slightly, which means that modulating the AOM frequency is an effective way of dithering the beam. It can also be shown that the diffraction efficiency is dependent on the intensity of the sound, meaning that changing the sound intensity changes the diffracted laser intensity, which is useful in our case as changing the laser intensity on the laser itself changes other beam properties (e.g. its waist size) as well.

2.3 Transport

Optical transport using focus-tuneable lenses was first demonstrated in [45] and was developed further in [47, 50].

To transport the atoms, we need to translate the focal point of the trapping beam (where the atoms are, in the ODT) along the optical axis. In principle, a focus displacement can be achieved using a single tuneable lens focusing a collimated beam. However, increasing the focal length increases the waist size as well, thereby changing trapping frequencies and trap depth during the transport. Instead of this, the system presented in Fig. 4 provides uniform trapping conditions over the full transport distance. This is preferable, since only strong confinement and large trap depth allow for fast transport. The two beams in Fig. 4(a) are focused behind the static lens L with focal length f at distances f (position A) and $2f$ (position B). Their waist sizes are equal if their divergences are. This requires beam diameters of d and $2d$ at L, respectively, resulting in the same divergence of $\theta = d/f$ for

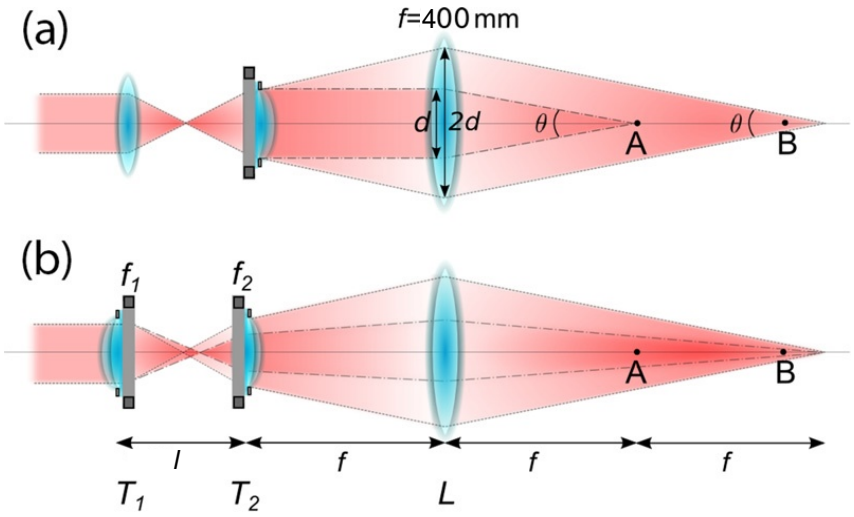

Figure 4. The system to dynamically control the size and position of a dipole trap. (a) Transport at constant beam waist over a distance f. If the separation between the tuneable lens T_2 and the static lens L equals the focal length f of the latter, the two beams can be transformed into each other by tuning f_2, while maintaining the same divergence $\theta = d/f$, thus the same waist size, between A and B. (b) Independent control over waist size and position of the focus. Replacing the first lens with a tuneable lens T_1 allows to change the beam size at T_2, resulting in a different divergence behind L. Illustration adapted from [45].

both. The beam focused at A must be collimated before the lens, and it can be shown that the beam focused at B must have the same divergence θ before passing L. Therefore, the two beams have the same size at a distance f before L. Placing a lens (let us call it T_2) with tuneable focus f_2 at this position allows continuous transformation of one beam into the other, resulting in a moving focus with constant waist.

This can also be shown using geometrical optics. By using the thin lens equation $1/f_2 = 1/t_2 + 1/k_2$ and using the fact that the incoming beam is collimated, so the object distance $t_2 = \infty$, we see the distance of the image created by T_2 is $k_2 = f_2$. If the incoming beam diameter is d the beam divergence after T_2 is $\theta_2 = d/k_2 = d/f_2$. Now, taking the other lens, the object distance will be $f - f_2$, so using $1/f = 1/(f - f_2) + 1/x_0$ results in an image distance $x_0 = f(f_2 - f)/f_2$. The diameter at f is $d_f = \theta_2(f - f_2)$ so the divergence after f is $\theta = d_f/x_0 = -d/f$ which is independent of f_2 as expected. This is all shown in Fig. 5.

The original system [45] uses a different version of the focus-tuneable lens (FTL), limiting $f_2 > 0$. Therefore, the divergence could only be reduced and the beam had to be focused before crossing T_2, as can be seen in Fig. 4(a), achieved by a static lens placed in front of T_2, which in turn defines the waist size behind L. In our case, the tuneable lens has a larger range and could also be set to produce $f_2 < 0$, meaning the beam does not have to be focused before T_2 in our case, which is useful to avoid power fluctuations caused by dust particles traversing the focal point. However, the same principle applies as in the original system, and in order to gain independent control over both the position and waist size of the focus, another tuneable lens T_1 is placed in front of T_2, as shown in the extended system in Fig. 4(b).

The system was modelled in Mathematica using ray transfer matrix analysis to see how

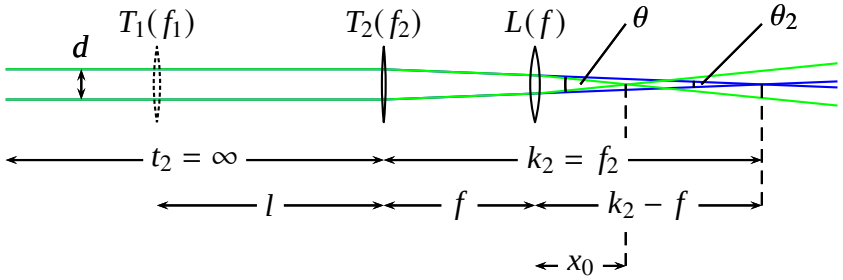

Figure 5. Schematics of the transport system. A collimated beam (object distance $t_2 = \infty$) with diameter $d = 2w_0$ enters the system and passes T_2, which focuses the beam to an image distance $k_2 = f_2$ with a divergence $\theta_2 = d/f_2$. This image distance means a virtual object distance of $-(k_2 - f)$ for the lens L since the distance between T_2 and L is f. Using the thin lens equation, we find the final image distance, the actual focus of our beam at $x_0 = f(f_2 - f)/f_2$ with a divergence $\theta = -d/f$. This is independent of f_2 as expected, so when f_2 is changed the beam waist is constant and transported. The position of T_1 is indicated in the figure but is not used for this calculation.

the laser beam propagates through the system enabling us to compute the waist size and the focus position for any focal length tuple (f_1, f_2). Ray transfer matrix analysis (also known as ABCD matrix analysis) is a type of ray tracing technique used in the design of some optical systems [51]. It involves the construction of a ray transfer matrix which describes the optical system; tracing of a light path through the system can then be performed by multiplying this matrix with a vector representing the light ray.

In the thin lens approximation, ray propagation over free space l and ray diffraction at a lens with focal length f can be described with the following ray transfer matrices:

$$\mathsf{P}_l = \begin{pmatrix} 1 & l \\ 0 & 1 \end{pmatrix}, \mathsf{L}_f = \begin{pmatrix} 1 & 0 \\ -1/f & 1 \end{pmatrix}. \tag{14}$$

The full system transfer matrix is then

$$\mathsf{S}_x = \mathsf{P}_x \mathsf{L}_f \mathsf{P}_f \mathsf{L}_{f_2} \mathsf{P}_l \mathsf{L}_{f_1}, \tag{15}$$

where x is the distance after L and l is the distance between T_1 and T_2. Let us now assume a Gaussian beam with waist size w_0, waist position z_0 and wavelength λ propagating through the system, along the optical axis (z direction). The complex beam parameter $q(z)$ is defined as

$$\frac{1}{q(z)} = \frac{1}{R(z)} - i\frac{\lambda}{\pi w(z)^2}, \tag{16}$$

where $R(z)$ is the radius of curvature of the beam and $w(z)$ is the beam's radius. From this, we immediately see that the beam radius is

$$w(z) = \sqrt{\frac{\lambda}{\pi \operatorname{Im}(-1/q(z))}}, \tag{17}$$

and the focus position is given by the condition

$$\operatorname{Re}(q(z)) = 0. \tag{18}$$

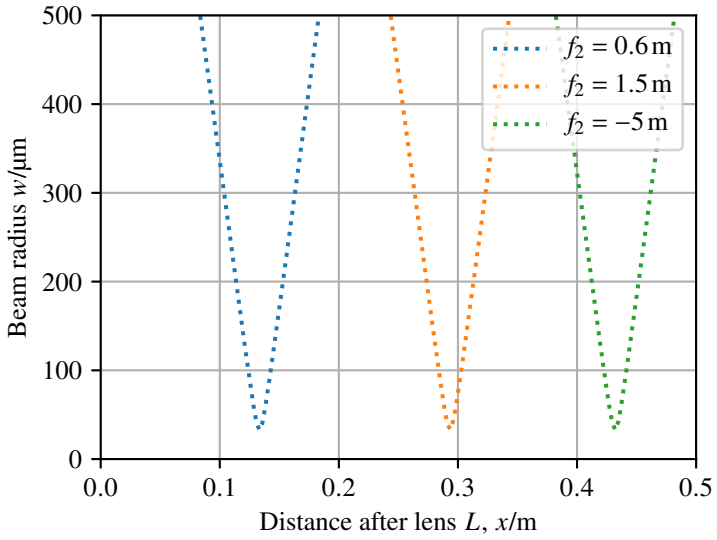

Figure 6. Ray trace of the proposed system after passing the static lens L with $l = 30\,\mathrm{cm}$, $f = 40\,\mathrm{cm}$, $w_0 = 4\,\mathrm{mm}$ and $\lambda = 1030\,\mathrm{nm}$. f_1 is set to infinity in this plot, so effectively that tuneable lens is switched off. We see the beam is focused after L. When f_2 is changed we see the beam waist w_x is constant and transported.

Now, assuming the incoming beam is collimated at T_1 with waist w, which we choose to be the origin of our coordinate-system, i.e. $z_0 = 0$ and so $R(0) = \infty$, the incoming beam parameter is

$$q_0 = i\frac{\pi w^2}{\lambda}. \tag{19}$$

Using the ray transfer equation

$$q_t = \frac{Aq_0 + B}{Cq_0 + D}, \tag{20}$$

where $\mathsf{S}_x = \begin{pmatrix} A & B \\ C & D \end{pmatrix}$ and this acts on the light vector proportional to $\begin{pmatrix} q_0 \\ 1 \end{pmatrix}$. We find in our case:

$$q_t = x - f + f^2\left(\frac{1}{f_2} + \frac{\pi w^2 + if_1\lambda}{(f_1 - l)\pi w^2 - if_1 l\lambda}\right). \tag{21}$$

We can use this to find the waist size at the trap w_0 and the focus position x_0 using Eqs. (17) and (18), respectively, as $w_0 = w(0)$:

$$w_0 = \frac{f|f_1|w\lambda}{\sqrt{(f_1 - l)^2(\pi w^2)^2 + (f_1\lambda l)^2}}, \tag{22}$$

$$x_0 = f - f^2\left(\frac{1}{f_2} + \frac{(f_1 - l)(\pi w^2)^2 - f_1^2\lambda^2 l}{(f_1 - l)^2(\pi w^2)^2 + (f_1\lambda l)^2}\right). \tag{23}$$

We see w_0 is independent of f_2 so it stays constant throughout the transport as expected. Also note that apart from the last term in x_0 which is a small Gaussian-ray correction, it is the same as we get from geometrical optics. A ray trace for our system can be seen in Fig. 6.

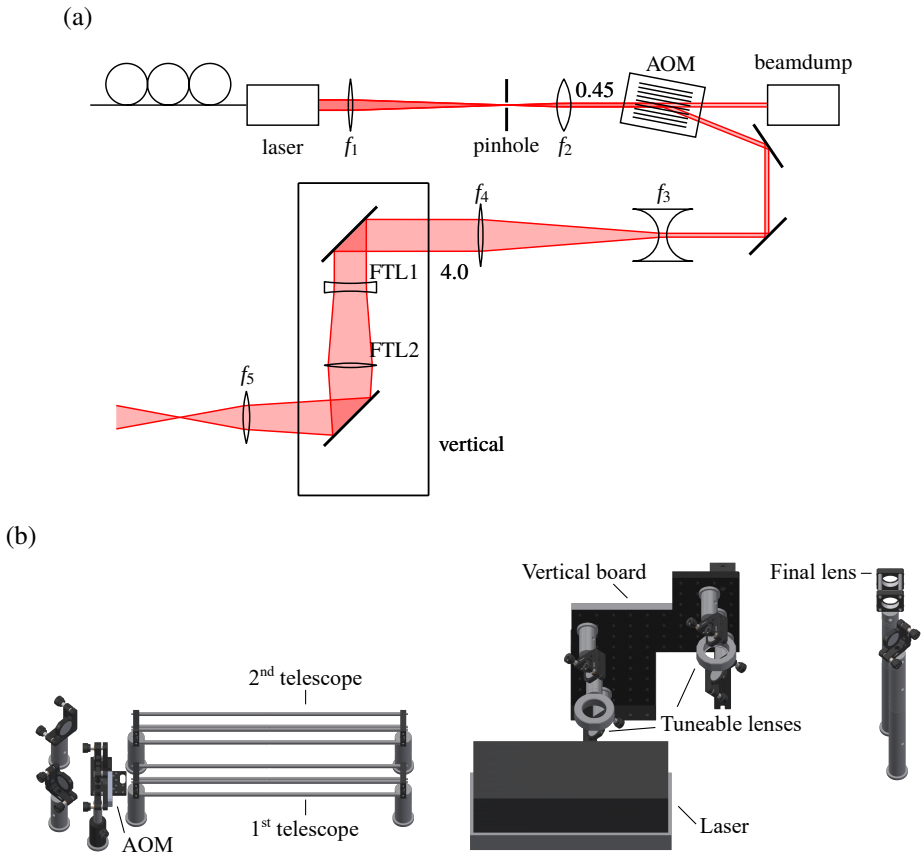

Figure 7. (a) Schematic view of the optical system for trapping and transporting the atoms. The beam is collimated to a 0.45 mm waist using a telescope (f_1 = 300 mm, f_2 = 100 mm) and a pinhole is used to filter out the so-called cladding modes. An AOM is used to deflect the beam and to control its power. Another telescope (f_3 = −50 mm, f_4 = 400 mm) is used to magnify the beam to a 4.0 mm waist. Two focus-tuneable lenses (arranged vertically) in conjunction with the final focusing lens (f_5 = 400 mm) allow control of the ODT size and position. (b) Realistic drawing of the transport system.

3 Experimental system

This project focused on designing and building the optical dipole trap (ODT) for trapping laser-cooled erbium atoms and the transport system for moving them approximately 50 cm to the science chamber. It builds on previous work undertaken earlier by this [36, 47] and other research groups [39, 45, 46, 49, 50].

The design process along with some initial tests is presented in Sec. 3.1 and results from the test setup can be found in Sec. 3.2.

3.1 System design

We first consider the required trap depth. Although the laser cooled atoms are at around 10 µK we expect some heating when compressing atoms into the ODT from the MOT. Atoms thermalise to approximately $1/10$ of the trap depth [52, 53], so we require a trap that is

several hundred µKs deep while maximising the spatial overlap with the MOT. The optimum trade-off between ODT size and depth is not known and may vary, for example, a large beam will probably optimise initial loading from the MOT but a smaller beam will be needed to ensure a large enough trapping frequency along the transport direction to avoid sloshing in the trap. Therefore, a scanning beam scheme is implemented to allow the ODT size to be dynamically tuned.

What is practically possible is also constrained by the laser power available. Although a wide range of wavelengths could be used for the ODT (see Fig. 2), given the availability of high power lasers and the fact that there is an issue with trapping the fermionic isotope ^{167}Er using the common ND:YAG laser at 1064 nm [39], it was decided that a 45 W, 1030 nm fibre laser[3] will be used [36]. The ODT and the transport uses the same laser beam.

The free parameters to match the requirements are the various lenses, distances and beam sizes in the transport setup and the ODT, giving a fairly large parameter space, but this is constrained by the clear aperture of the FTLs and the AOM used to dither the beam and to control its power. The system devised gives a trap depth of 655 µK and trapping frequencies $\omega_{x,y} = 1.73\,\text{kHz}, \omega_z = 12.2\,\text{Hz}$ and can be seen in Fig. 7. Below we describe the process that lead to create this system.

First of all, the beam properties of the laser had to be measured. As shown in Fig. 8(a) we found that the beam fits a Gaussian propagation model well. However, it is important to note that the beam waist and its position changes considerably when the output power on the laser is varied (see Fig. 8(b) and (c)), so all measurements presented in this report correspond to using the laser at the highest output power (45 W), as we need all the power to create a deep enough ODT. We also found that there are some so-called cladding modes present which can make the beam doughnut-shaped close to its focus. This issue was solved by putting an iris at the focal point of the first telescope (see Fig. 7).

Next, we had to pick a beam radius w_0 incident on the first FTL and a value for the final fixed focal length lens f and the distance between the two tuneable lens l. The original transport system [45] was slightly modified [47, 50] to use a different version of the tuneable lenses[4] capable of producing a wider range of focal lengths. These lenses were tested during two master's projects [47, 50] to see how stable they are, to what extent they tolerate heating and how quickly they settle at the focal length set. It was found that the lenses work sufficiently well, but they have to be used with their optical axis being vertical and that thermal drifts need to be compensated. A basic test setup was built in both cases, but these needed to be redesigned to match the requirements (trap depth, transport length) of our experiment.

Regarding trapping conditions, we have to load the ODT 10 cm away from the final lens that is mounted right next a the viewport of the vacuum chamber, and we have to achieve a beam waist that results in a trap depth that is several hundred µKs deep. We then have to transport our atoms into the glass 'science cell' 50 cm away from the final lens. We also have to make sure that our beam is small enough so that it can go through the tuneable lenses (clear aperture 16 mm) and need to keep in mind that their range is $-2\,\text{m}^{-1} < 1/f_{1,2} < 3\,\text{m}^{-1}$.

To explore the parameter space, multiple plots like $U_0(w_0, f_1), x_0(w_0, f_1), x_0(f, l)$

[3] ALS-IR-1030-50-I-SF, from Azure Light Systems.

[4] EL-16-40-TC-VIS-5D, from Optotune.

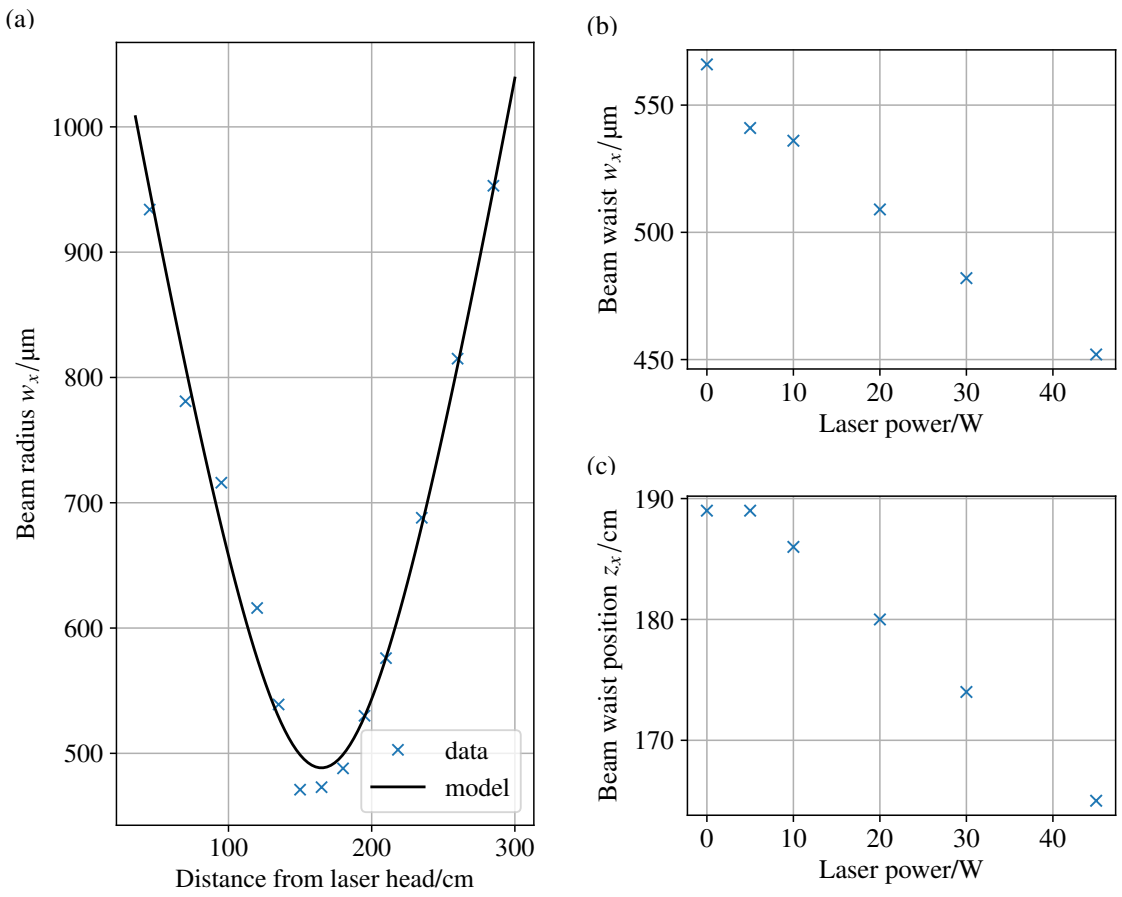

Figure 8. (a) Plot of the Gaussian beam radius against distance from the laser head. The data fits the Gaussian propagation model well. The fitted beam waist is $w_{x,0} = 488(22)$ µm and the waist position is $z_{0,x} = 165(3)$ cm, measured from the laser head. (b) Beam waist against the laser power. It can be seen that the waist changes by more than 100 µm when the laser power is turned all the way up. (c) Beam waist position measured from the laser head, against the laser power. It can be seen that the waist position changes by around 25 cm when the laser power is turned all the way up.

and $x_0(f, f_2)$ were created. The laser power is 45 W, so 30 W was used throughout the calculations to account for losses (e.g. the reflection from optical elements or the limited AOM diffraction efficiency), to be on the safe side. The polarisability was taken to be $\alpha = 166$ a.u. $= 2.74 \times 10^{-39}$ C m^2 V^{-1} [26]. It was found that the combination $l = 30$ cm, $f = 40$ cm, $w_0 = 4$ mm would mean that when T_1 is switched off, we get a trap that is 655 µK deep (33 µm waist) and that we can transport the atoms by tuning $-1\,\mathrm{m}^{-1} < 1/f_2 < 2\,\mathrm{m}^{-1}$. Using a large part of the available range of f_2 is useful as the focus position will be less sensitive to fluctuations in f_2. By tuning $-1.1\,\mathrm{m}^{-1} < 1/f_1 < 1.1\,\mathrm{m}^{-1}$ we can still transport the atoms over the whole distance but can change the trap waist $25\,\mu\mathrm{m} < w < 50\,\mu\mathrm{m}$. This in turn changes the trap depth, which can also be changed by changing the power in the beam using the AOM. The incoming beam waist is also ideal as it is small enough so that there will be no clipping, meaning no power loss or beam profile corruption, but large enough to be able to focus it tightly.

Finally, the dithering system had to be designed. A telescope makes the beam size small

enough to fit into the AOM. Finding the right magnification took multiple rounds, as it turned out that the active aperture of the AOM is considerably smaller than specified (1.25 mm), meaning that the top and the bottom of the beam is not deflected, resulting in an elliptical beam in the first order. We now use an incoming beam diameter of 0.9 mm which still results in a slightly elliptic beam, but we did not want to make the beam smaller fearing it would compromise our diffraction efficiency and hence the power in the ODT. We also made this telescope to deliberately focus the beam, to filter the cladding modes with a pinhole around the focus as these modes are highly divergent. Virtually no power loss through the pinhole was measured at high powers. It is also important to mention that the telescope was designed to collimate the incoming laser beam, which is otherwise convergent.

We then calculated how much we can dither the beam by to be able to trap as many atoms as possible while maintaining a sufficient trap depth and avoiding any clipping on the lenses. Turning again to the ABCD formalism, we know

$$\begin{pmatrix} r \\ \varphi \end{pmatrix} = \mathsf{S}_{\text{system}} \begin{pmatrix} r_0 \\ \varphi_0 \end{pmatrix}, \tag{24}$$

where $r_{(0)}$ is the (initial) distance of the beam from the optical axis, $\varphi_{(0)}$ is the (initial) angle the beam makes with the optical axis and $\mathsf{S}_{\text{system}}$ is the ABCD matrix describing the whole system after the AOM (i.e. the telescope magnifying the beam and the transport system). We know $r_0 = 0$, and so by substituting our values to get $\mathsf{S}_{\text{system}}$ we get $\begin{pmatrix} r \\ \varphi \end{pmatrix} \approx \begin{pmatrix} 0.05\,\text{m}\,\varphi_0 \\ -6\varphi_0 \end{pmatrix}$.

Without clipping we can dither the beam such that its waist becomes three times as big as the original (i.e. increasing w_x to 100 µm, with a MOT approximately 1000 µm wide). As we know $w_0 = 33$ µm, we would like to have $r \approx 100$ µm meaning $\varphi_0 = 0.1°$. Using Eq. (13) we find $\Delta f_{\text{AOM}} = 15$ MHz for our AOM. As the central frequency of our AOM is $f_0 = 110$ MHz we see Δf_{AOM} is doable. We also see the maximum beam angle at the ODT $\varphi = 0.6°$ will not be too large, and the beam will be dithered roughly parallel to itself.

From a more technical point of view, the telescopes were designed to have one convex and one concave lens each to avoid focusing a high-power beam which could lead to power fluctuations if something gets in the focus. The lenses were put in a cage system and built using fixed height posts to minimise the necessary alignment. The whole experiment including the FTLs and the AOM is computer controlled through National Instruments cards[5], for which a breakout box was designed and built to be able to communicate via BNC cables. From the software side, the experiment is controlled using the Cicero sequence generator[6], communicating with the NI chassis. It is proposed that the dithering sequence will be controlled via an FPGA chip[7], but this is still under development. For testing purposes, dithering was controlled via a signal generator.

3.2 Test setup

After this design process, a test setup was built to see how well it can maintain a constant waist over transport and how any drifts can be compensated. The AOM and the dithering

[5]NI PXIe-6733, NI PXIe 6738 and NI PXIe-6536.

[6]Created by Aviv Keshet, available at http://akeshet.github.io/Cicero-Word-Generator/.

[7]STEMlab 125-10 from Red Pitaya.

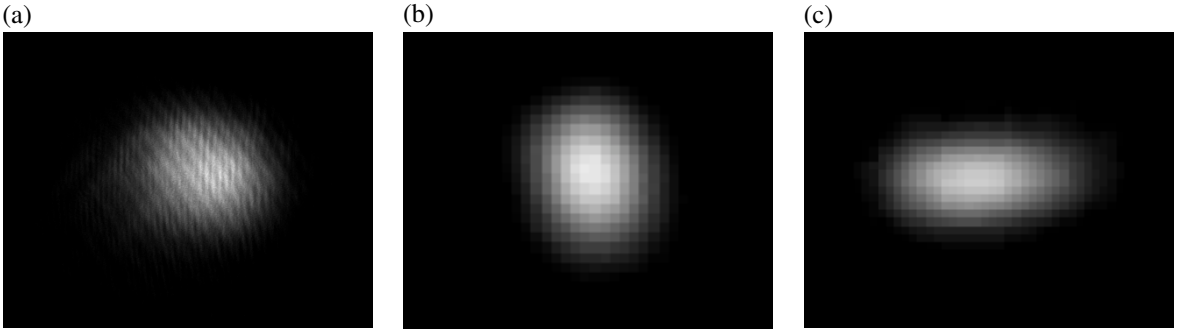

Figure 9. Beam images from the test system. (a) The first order beam after the AOM. An elliptic beam can be seen with $w_x = 450\,\mu\text{m}$, $w_y = 360\,\mu\text{m}$ ($w_x/w_y = 1.25$), but the beam is otherwise Gaussian. The fringes are an imaging artefact. (b) The undithered trapping beam focused near the MOT position. The beam is Gaussian with beam waist $w_{x,0} = 44\,\mu\text{m}$, $w_{y,0} = 53\,\mu\text{m}$. (c) Dithered beam with a dithering amplitude $A = 2.6w_{x,0}$. The beam remains Gaussian, with an increased beam waists $w_x = 121\,\mu\text{m}$, $w_y = 54\,\mu\text{m}$.

also needed to be tested, to see if they match the design parameters. There were some rather confusing problems caused by the high-power beam and the tuneable lens during building the test setup, and identifying the source of the curious beam shapes and circumventing the problems took a significant amount of time. High power imaging techniques along with beam quality quantisation are presented in Sec. A.

Regarding the AOM, the first order beam is used to be able to dither the beam via modulating the AOM frequency and to control its power via the RF power (the zeroth order is picked off and dumped). 2 % insertion loss and 92 % diffraction efficiency were measured when the AOM was driven at its centre frequency (110 MHz), which is slightly better than the specifications of the device (4 % and 90 %, respectively). It is important to note that the AOM distorts the circular beam to be slightly elliptic, with its major axis becoming 25 % larger than its minor axis. The beam was focused down to 450 µm waist (instead of the specified aperture radius of 625 µm) using a telescope to decrease the ellipticity, but was not decreased further fearing it would compromise the diffraction efficiency resulting in a smaller power in the ODT. An image can be seen in Fig. 9.

After this, a second telescope was built, which increases the beam waist to 4.0 mm. While beam sizes were usually measured by imaging them with a camera and then fitting a Gaussian on top, as this beam was too wide to image its waist was measured by moving a knife-edge through the beam.

The two focus-tuneable lenses were then inserted. Due to heating up, while the beam shape remains Gaussian for the first 2.5 s, a focal length drift can still be seen. The lenses' optical power $D = {}^1/_f$ could be set via applying a DC voltage to their driver so a focal-length drift can be compensated by applying a variable voltage. The lenses were set to focus at the atoms' final position, and the focus position drift rate was measured by imaging the beam along its focus for 5 s and then finding the focus position $x_0(t)$. Without compensation, a constant drift rate of $2.5(1)\,\text{mm}\,\text{s}^{-1}$ could be seen, while with compensation on, this could be brought down to $0.25(6)\,\text{mm}\,\text{s}^{-1}$. For this, a compensation rate $\dot{D} = 0.016\,\text{m}^{-1}\,\text{s}^{-1}$ need to be used. The same measurement was carried out close to the MOT position and the same

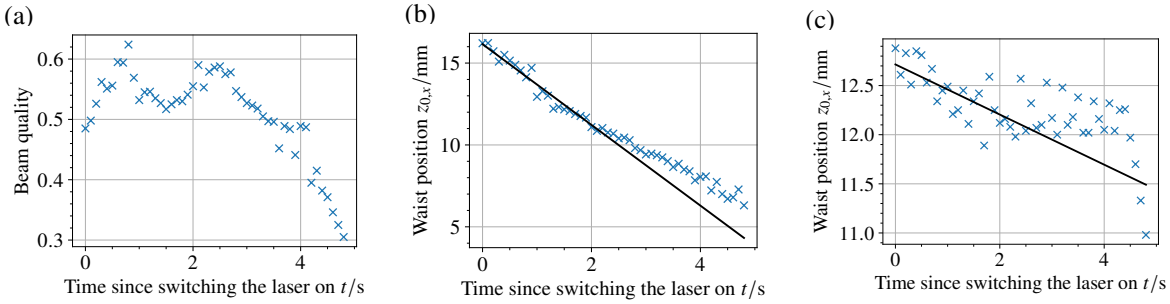

Figure 10. Results from the tuneable lens testing. (a) Beam quality as a function of time elapsed after shining light on the lenses. We see it remains roughly constant for 2.5 s after which it decreases indicating a significant distortion of the beam shape. The beam quality number is discussed in Sec. A. (b) The ODT position measured on a translation stage as a function of time, with no compensation. A fitted drift rate of 2.5(1) mm s^{-1} can be seen. (c) The ODT position measured on a translation stage as a function of time, compensation on. A much smaller fitted drift rate of 0.25(6) mm s^{-1} can be seen.

final drift rate was achieved using the same compensation rate. The constant waist transport was also tested. At the MOT position the beam waist was $w_{y,\mathrm{MOT}} = 44\,\mu\mathrm{m}$, at the final position the beam waist was $w_{y,\mathrm{final}} = 48\,\mu\mathrm{m}$. This is a 9 % increase which we attribute to non-perfect alignment that we hope to correct in the final setup. Results can be seen in Fig. 10.

Finally, the dithering was tested. We needed to make sure that the beam is dithered much faster than the relevant trapping frequency, $\omega_x = 1.73\,\mathrm{kHz}$, to avoid parametric heating of our atoms. However, we cannot dither the beam arbitrarily fast, as high-frequency dithering (i.e. high-frequency modulation of the AOM frequency) is limited by how quickly the AOM driver can respond to frequency modulation. By dithering the beam at constant amplitude, but at different frequencies, we found we can dither the atoms at a frequency of up to 50 kHz, which is fast enough. We also needed to test how well the resulting trapping potential matches the theory. As the resulting trap is not exactly Gaussian, there is no analytic formula to express the waist size as a function of the dithering amplitude. However, we can always fit a Gaussian to it, and take its waist as the expected beam waist. We found very good agreement with the theory, the dithered trapping potentials were Gaussian and the resulting beam waists were close to expected. Results can be seen in Fig. 11.

4 Conclusions and Outlook

4.1 Conclusions

An all-optical system using focus-tuneable lenses to trap and transport ultracold erbium atoms was designed, constructed and tested. The system designed can trap atoms with a trap depth of 655 µK and can transport them over 50 cm. The size of the trap can be varied between 25 µm and 50 µm. The test setup achieves a waist size $w_{x,0} = 44\,\mu\mathrm{m}$. Time-averaged potentials were also introduced using an acousto-optic modulator (AOM) and we found we can dither the beam at up to a 50 kHz rate above which the AOM driver cannot follow the

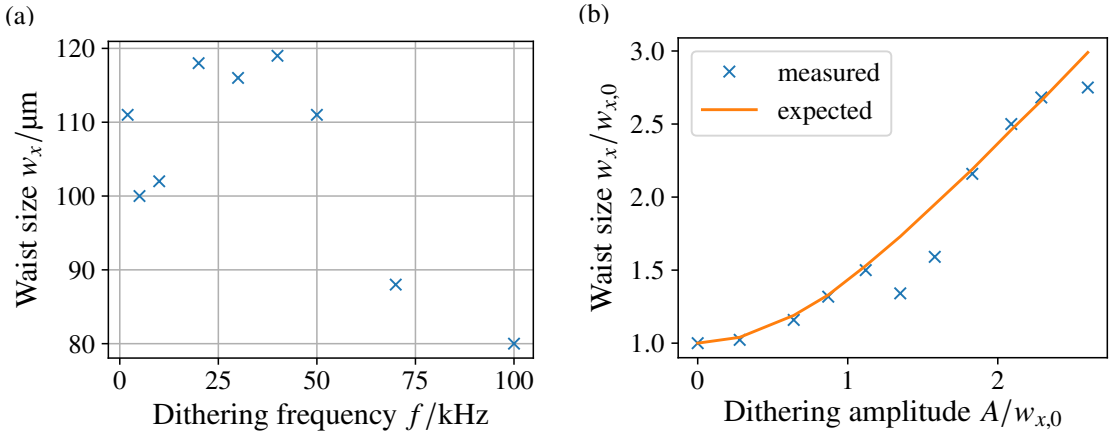

Figure 11. Results from the dithering tests. (a) Waist size against the dithering frequency, at constant dithering amplitude of $A = 2.6w_x$. A significant reduction in waist size can be seen for frequencies over 50 kHz, indicating that the AOM driver cannot respond to such high-frequency modulation. (b) Waist size against dithering amplitude, at constant dithering frequency of 20 kHz. The resulting beam waists match the expected waists well.

driving frequency modulation. This could make the waist up to three times as large as the original (we measured $w_x = 121$ µm with the test setup) and the resulting trap widths match the theoretical values well. The results so far look promising regarding the viability of the system proposed for the optical dipole trap and for transport.

4.2 Next steps & future directions

The final version of the system is currently being integrated with the rest of the experiment. Once we have a MOT with suitably large atom numbers the ODT loading efficiency and the trap depth will be tested and optimised using the tuneability designed in the system. The atoms can then be evaporatively cooled which will be followed by testing the transport efficiency, i.e. how many atoms we lose throughout the transport, which will also involve optimising the transport sequence to find out what the velocity of the trap $v(t)$ should be throughout the transport to lose the least atoms but also maintain their low temperature. The atoms will finally be loaded into a quasi-2D optical box (see Fig. 12) generated from a red-detuned sheet-beam and a blue-detuned wall, created with a spatial light modulator (SLM). The SLM setup is currently being designed and tested.

Having the atoms condensed and loaded into the optical box brings us to the point at which we can start with long-term research work on both the equilibrium and non-equilibrium properties of the dipolar Bose gas. More details of our specific plans are given in my Project Initiation Plan.

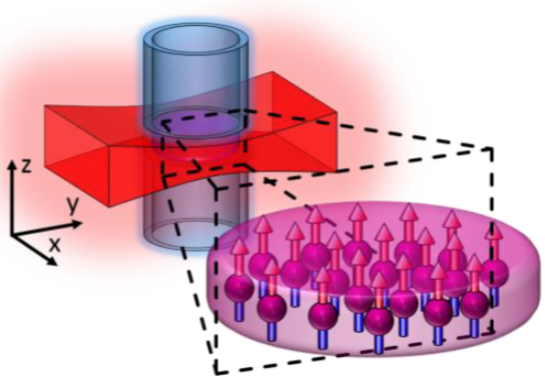

Figure 12. Polarized gas of erbium atoms captured in a 2D box potential. The potential is created with a red-detuned sheet-beam and a blue-detuned wall, created with an SLM. The atoms are polarized due to a magnetic bias field.

Acknowledgements

The author would like to thank Dr Anna Marchant, Milan Krstajic and Lucas Hofer for the relevant discussions and day-to-day help and Dr Robert Smith for the overall guidance of this project.

Appendix

A High-power beams

Most of our optics and devices were not prepared to bear such high powers and intensities that we use. In fact, another group have already abandoned using the same type of lenses and switched to fixed focal length lenses made of a different material (UV fused silica instead of N-BK7, as the former has a lower thermal expansion coefficient, causing a smaller thermal lensing effect) and also decided to use a transport system with lenses on a translation stage instead of the focus-tuneable lenses (FTLs) precisely because they do not operate well under high power [54].

This was not easy to foresee as the FTLs have a damage threshold that is much higher than the laser intensities we use. In line with this, the lenses are not permanently damaged in our setup but show very significant thermal lensing, meaning they can only be used during the first few seconds after the laser light reached them and then they need to be left cooling for around 30 s. On top of this, these lenses have to be used with their optical axes vertical. This is not ideal, but in our experimental sequence we will only have high power on the lenses for a short time, so we are going ahead with this solution. Regarding the fixed focal length lenses, using N-BK7 lenses made by Thorlabs seemed suitable in our case, and no difference could be seen when lenses made of UV fused silica were substituted for lenses made of N-BK7.

Another problem with characterising our setup was imaging high intensities (e.g. the ODT at full power) as most intensity filters break at such high powers and cubes do not work perfectly either.

These problems were not straightforward to circumvent, and the high power imaging techniques are presented in Sec. A.1 along with beam quality quantisation are presented in Sec. A.2. A few images of the various problems are presented in Fig. 13.

A.1 High-power beam imaging

It was not straightforward to image a 45 W beam, given this is too much for a camera and no filter can take such high power. As the filters can take up to 10 mW at the beam waists we use, we need to filter out as much as 99.98 % of the light. Traditionally, to achieve this, a combination of a half-wave plate placed in front of a polarising beamsplitter cube is used. The waveplate rotates the polarisation of the light which is then split by the cube, so by rotating the waveplate the transmitted light intensity can be controlled. In our case, the cube transmits horizontally polarised light, and since the laser polarisation is vertical it has to be rotated by only a very small amount to get suitably low power in the transmitted wave.

The problem with this, and this took quite some time to figure out, is that there is a horizontally polarised part of the laser light that has a strange pattern, which then also gets transmitted through the cube. While the power in this originally horizontal part (power $H = 40$ mW) is much smaller than that of the vertical part (power $V = 45$ W), it is comparable to the transmitted portion of the vertical part we really want to look at, and so we observe a pattern that is really not Gaussian (c.f. Fig. 13(b)). We also tried to image the beam by trying

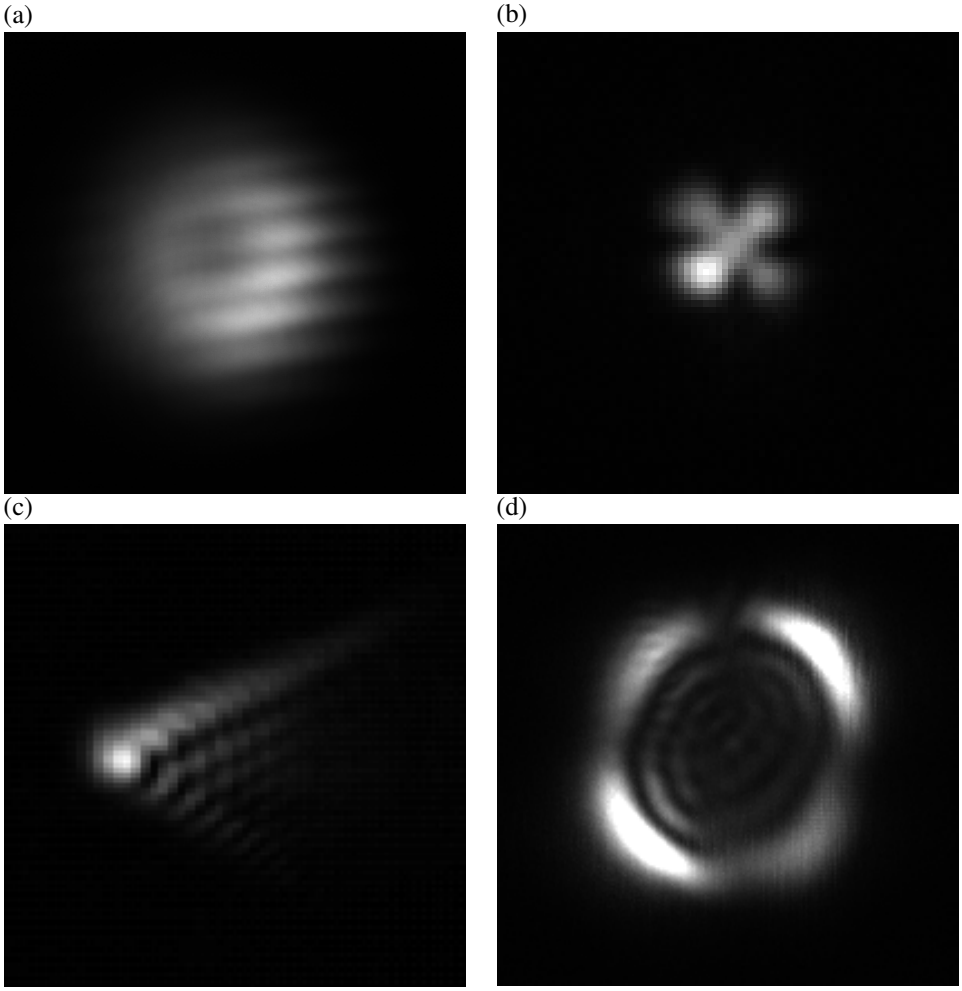

Figure 13. Different issues with the laser beam during initial testing. (a) The beam coming out of the laser near its waist. The beam is doughnut-shaped, due to cladding modes present. A Gaussian shape can be restored by filtering these modes out, putting an iris at the focus. (b) Problems with high-power beam imaging. This beam shape is an imaging artefact, caused by internal reflections and the finite extinction ratio when a cube and waveplate is used to reduce the power to image the beam. The solution to circumvent this is presented in Sec. A. (c) Comatic aberration when the focus-tuneable lens is used with the optical axis horizontal. This can be solved by turning the lens to have its optical axis vertical. (d) Thermal lensing, caused by the heating up of the focus-tuneable lens. A severely distorted beam shape develops over 5 s, so the lens can only be used for a few seconds after which is needs to cool down, taking 30 s.

to look at the transmitted part through a back-polished mirror, but this was not successful as the transmission ratio was too low.

The solution is to introduce a beam sampler between the waveplate and the cube. To get the smallest amount of light through the system we need to look at the p-polarised (i.e. horizontal) light as the reflectance of the beam sampler is much smaller for p-polarisation than it is for s-polarisation (i.e. vertical). The idea then is that we turn the waveplate so it rotates the polarisation of the laser by 90°, so a small part of V and a larger part of H is reflected. This is not a problem, since $V \gg H$, and so the cube will now be able to filter out

the H part which is now vertical, enabling us to look at the transmitted V part.

Mathematically, if the waveplate rotates the polarisation by θ, the power in the horizontal part of the beam after the waveplate (p-polarisation) will be $P_p = V\sin^2(\theta) + H\cos^2(\theta)$, while in the new vertical part (s-polarisation) it will be $P_s = V\cos^2(\theta) + H\sin^2(\theta)$. If the reflection coefficients for the two polarisations are R_p and R_s, with $R_s \gg R_p$, the total reflected power is $P = R_pP_p + R_sP_s$. Due to the large power imbalance between the p and the s part, we have to take into account the finite extinction ratio of the cube, e. Assuming a horizontal transmittance close to 1, the total power transmitted through the cube is $P_t = R_pP_p + \frac{1}{e}R_sP_s$. $R_{p,s}$ are a function of the angle of incidence θ_i of the laser on the beam sampler and the refractive index of the beam sampler n:

$$R_p = \left| \frac{\sqrt{1 - \left(\frac{\sin(\theta_i)}{n}\right)^2} - n\cos(\theta_i)}{\sqrt{1 - \left(\frac{\sin(\theta_i)}{n}\right)^2} + n\cos(\theta_i)} \right|^2, \tag{25}$$

$$R_s = \left| \frac{n\sqrt{1 - \left(\frac{\sin(\theta_i)}{n}\right)^2} - \cos(\theta_i)}{n\sqrt{1 - \left(\frac{\sin(\theta_i)}{n}\right)^2} + \cos(\theta_i)} \right|^2. \tag{26}$$

In theory, we can then make P_s arbitrarily small by adjusting θ_i, but for our model of beam sampler[8] we see the smallest we can make R_p is 0.0022 % with $R_s \approx 1000R_p$ at the same angle. We also see that the extinction ratio for the transmitted beam of our cube[9] is $e \approx 1000$.

If $\theta = 0°$, the transmitted power is $P_0 = R_pH + \frac{1}{e}R_sV$, whereas if $\theta = 90°$, the transmitted power is $P_{90} = R_pV + \frac{1}{e}R_sH$. These are roughly equal, as substituting the known ratios we get $P \approx R_p(V+H)$ in both cases, which was confirmed by measurement. Since $V/H \approx 1000$, we get $P \approx R_pV$, so we can look at only the V part in both cases. However, we prefer to look at the $\theta = 90°$ case as then we can look at a directly transmitted V part rather than relying on it being transmitted due to the non-perfect finite extinction ratio of the cube.

With this technique we can get rid of all the high-power imaging artefacts. The system can be seen in Fig. 14.

A.2 Beam quality

Due to observing many different, non-Gaussian patterns, we had to devise a metric describing how close our beam is to a perfect Gaussian. While there are many different ways to do this, what we are really interested in is how well trapping will work, i.e. how high the peak intensity is of the beam compared to a Gaussian beam with the same total power.

To measure the peak intensity, we look at our beams with a camera with square pixels of

[8] BSF10-B, from Thorlabs.

[9] CCM1-PBS253/M, from Thorlabs.

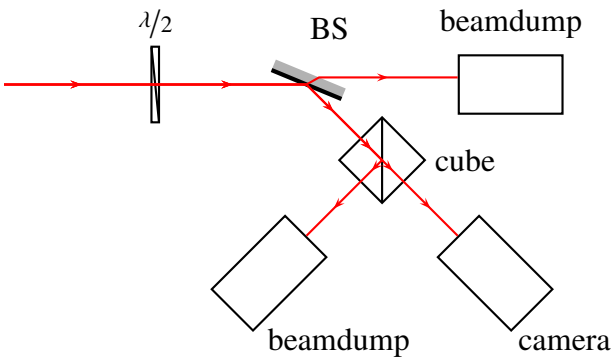

Figure 14. The system to image the high-power beam. The beam goes through a waveplate rotating its polarization by $\theta = 90°$ and then reflects from a beam sampler (BS) at roughly $\theta_i = 55°$ angle of incidence. It then goes through a polarising beam splitter cube so the horizontal polarization is kept and then it is imaged with a camera.

size a. The intensity distribution of a Gaussian beam is:

$$I(x, y) = I_0 e^{-\frac{2x^2}{w_x^2} - \frac{2y^2}{w_y^2}}, \tag{27}$$

where I_0 is the peak intensity and $w_{x,y}$ are its waists. Now, the brightness of each pixel depends on the power incident on the pixel, and at the central pixel we will record a power of

$$P_c = \int_{-\frac{a}{2}}^{\frac{a}{2}} \int_{-\frac{a}{2}}^{\frac{a}{2}} I(x, y)\, \mathrm{d}x\, \mathrm{d}y = \frac{1}{2} I_0 \pi w_x w_y \operatorname{erf}\left(\frac{a}{\sqrt{2} w_x}\right) \operatorname{erf}\left(\frac{a}{\sqrt{2} w_y}\right). \tag{28}$$

The total power in the beam is

$$P_0 = \int_{-\infty}^{\infty} \int_{-\infty}^{\infty} I(x, y)\, \mathrm{d}x\, \mathrm{d}y = \frac{1}{2} I_0 \pi w_x w_y, \tag{29}$$

so the relative power on the central pixel compared to the total power for a perfectly Gaussian beam is

$$P_{\mathrm{rel}} = \frac{P_c}{P_0} = \operatorname{erf}\left(\frac{a}{\sqrt{2} w_x}\right) \operatorname{erf}\left(\frac{a}{\sqrt{2} w_y}\right). \tag{30}$$

For the imaged beam, we can record the total power by summing all pixel values. To get the central power, we can select the brightest pixel and claim it is the centre of the beam where atoms will be trapped, or if the beam is reasonably Gaussian, we can also fit a Gaussian to it and extract the peak power from that. The ratio of these two will be the experimentally measured $P_{\mathrm{rel,\,exp}}$ which we can compare to the theoretical P_{rel} we expect, and create the metric

$$I_{\mathrm{rel}} = \frac{P_{\mathrm{rel,\,exp}}}{P_{\mathrm{rel}}}. \tag{31}$$

If $I_{\mathrm{rel}} \approx 1$ it means the peak intensity is close to what we expect of a Gaussian beam, if $I_{\mathrm{rel}} < 1$ it means the peak intensity is smaller than what we would like to see.

References

[1] A. D. Cronin, J. Schmiedmayer and D. E. Pritchard, 'Optics and interferometry with atoms and molecules', Rev. Mod. Phys. **81**, 1051 (2009).

[2] C. Gross, T. Zibold, E. Nicklas, J. Estève and M. K. Oberthaler, 'Nonlinear atom interferometer surpasses classical precision limit', Nature **464**, 1165 (2010).

[3] B. T. Seaman, M. Krämer, D. Z. Anderson and M. J. Holland, 'Atomtronics: Ultracold-atom analogs of electronic devices', Phys. Rev. A **75**, 023615 (2007).

[4] I. Bloch, J. Dalibard and S. Nascimbène, 'Quantum simulations with ultracold quantum gases', Nat. Phys. **8**, 267 (2012).

[5] A. L. Gaunt, T. F. Schmidutz, I. Gotlibovych, R. P. Smith and Z. Hadzibabic, 'Bose-Einstein Condensation of Atoms in a Uniform Potential', Phys. Rev. Lett. **110**, 200406 (2013).

[6] N. Navon, A. L. Gaunt, R. P. Smith and Z. Hadzibabic, 'Critical dynamics of spontaneous symmetry breaking in a homogeneous Bose gas', Science **347**, 167 (2015).

[7] C. Eigen, A. L. Gaunt, A. Suleymanzade, N. Navon, Z. Hadzibabic and R. P. Smith, 'Observation of Weak Collapse in a Bose-Einstein Condensate', Phys. Rev. X **6**, 041058 (2016).

[8] N. Navon, A. L. Gaunt, R. P. Smith and Z. Hadzibabic, 'Emergence of a turbulent cascade in a quantum gas', Nature **539**, 72 (2016).

[9] A. Griesmaier, J. Werner, S. Hensler, J. Stuhler and T. Pfau, 'Bose-Einstein Condensation of Chromium', Phys. Rev. Lett. **94**, 160401 (2005).

[10] K. Aikawa, A. Frisch, M. Mark, S. Baier, A. Rietzler, R. Grimm and F. Ferlaino, 'Bose-Einstein Condensation of Erbium', Phys. Rev. Lett. **108**, 210401 (2012).

[11] M. Lu, N. Q. Burdick, S. H. Youn and B. L. Lev, 'Strongly Dipolar Bose-Einstein Condensate of Dysprosium', Phys. Rev. Lett. **107**, 190401 (2011).

[12] T. Lahaye, C. Menotti, L. Santos, M. Lewenstein and T. Pfau, 'The physics of dipolar bosonic quantum gases', Rep. Prog. Phys. **72**, 126401 (2009).

[13] A. Bühler and H. P. Büchler, 'Supersolid phase in atomic gases with magnetic dipole interaction', Phys. Rev. A **84**, 023607 (2011).

[14] L. Tanzi, E. Lucioni, F. Famà, J. Catani, A. Fioretti, C. Gabbanini, R. N. Bisset, L. Santos and G. Modugno, 'Observation of a Dipolar Quantum Gas with Metastable Supersolid Properties', Phys. Rev. Lett. **122**, 130405 (2019).

[15] F. Böttcher, J.-N. Schmidt, M. Wenzel, J. Hertkorn, M. Guo, T. Langen and T. Pfau, 'Transient Supersolid Properties in an Array of Dipolar Quantum Droplets', Phys. Rev. X **9**, 011051 (2019).

[16] L. Chomaz, D. Petter, P. Ilzhöfer, G. Natale, A. Trautmann, C. Politi, G. Durastante, R. M. W. van Bijnen, A. Patscheider, M. Sohmen, M. J. Mark and F. Ferlaino, 'Long-Lived and Transient Supersolid Behaviors in Dipolar Quantum Gases', Phys. Rev. X **9**, 021012 (2019).

[17] G. Natale, R. M. W. van Bijnen, A. Patscheider, D. Petter, M. J. Mark, L. Chomaz and F. Ferlaino, 'Excitation Spectrum of a Trapped Dipolar Supersolid and Its Experimental Evidence', Phys. Rev. Lett. **123**, 050402 (2019).

[18] M. Guo, F. Böttcher, J. Hertkorn, J.-N. Schmidt, M. Wenzel, H. P. Büchler, T. Langen and T. Pfau, 'The low-energy Goldstone mode in a trapped dipolar supersolid', arXiv e-prints, arXiv:1906.04633 (2019).

[19] M. Boninsegni and N. V. Prokof'ev, 'Colloquium: Supersolids: What and where are they?', Rev. Mod. Phys. **84**, 759 (2012).

[20] H. Kadau, M. Schmitt, M. Wenzel, C. Wink, T. Maier, I. Ferrier-Barbut and T. Pfau, 'Observing the Rosensweig instability of a quantum ferrofluid', Nature **530**, 194 (2016).

[21] I. Ferrier-Barbut, H. Kadau, M. Schmitt, M. Wenzel and T. Pfau, 'Observation of Quantum Droplets in a Strongly Dipolar Bose Gas', Phys. Rev. Lett. **116**, 215301 (2016).

[22] L. Chomaz, S. Baier, D. Petter, M. J. Mark, F. Wächtler, L. Santos and F. Ferlaino, 'Quantum-Fluctuation-Driven Crossover from a Dilute Bose-Einstein Condensate to a Macrodroplet in a Dipolar Quantum Fluid', Phys. Rev. X **6**, 041039 (2016).

[23] L. Santos, G. V. Shlyapnikov and M. Lewenstein, 'Roton-Maxon Spectrum and Stability of Trapped Dipolar Bose-Einstein Condensates', Phys. Rev. Lett. **90**, 250403 (2003).

[24] L. Chomaz, R. M. W. van Bijnen, D. Petter, G. Faraoni, S. Baier, J. H. Becher, M. J. Mark, F. Wächtler, L. Santos and F. Ferlaino, 'Observation of roton mode population in a dipolar quantum gas', Nat. Phys. **14**, 442 (2018).

[25] D. Petter, G. Natale, R. M. W. van Bijnen, A. Patscheider, M. J. Mark, L. Chomaz and F. Ferlaino, 'Probing the Roton Excitation Spectrum of a Stable Dipolar Bose Gas', Phys. Rev. Lett. **122**, 183401 (2019).

[26] J. H. Becher, S. Baier, K. Aikawa, M. Lepers, J.-F. Wyart, O. Dulieu and F. Ferlaino, 'Anisotropic polarizability of erbium atoms', Phys. Rev. A **97**, 012509 (2018).

[27] R. P. Feynman, 'Atomic Theory of the Two-Fluid Model of Liquid Helium', Phys. Rev. **94**, 262 (1954).

[28] S. Moulder, S. Beattie, R. P. Smith, N. Tammuz and Z. Hadzibabic, 'Quantized supercurrent decay in an annular Bose-Einstein condensate', Phys. Rev. A **86**, 013629 (2012).

[29] R. Desbuquois, L. Chomaz, T. Yefsah, J. Léonard, J. Beugnon, C. Weitenberg and J. Dalibard, 'Superfluid behaviour of a two-dimensional bose gas', Nat. Phys. **8**, 645 (2012).

[30] A. Filinov, N. V. Prokof'ev and M. Bonitz, 'Berezinskii-Kosterlitz-Thouless Transition in Two-Dimensional Dipole Systems', Phys. Rev. Lett. **105**, 070401 (2010).

[31] B. Kain and H. Y. Ling, 'Polarons in a dipolar condensate', Phys. Rev. A **89**, 023612 (2014).

[32] N. B. Jørgensen, L. Wacker, K. T. Skalmstang, M. M. Parish, J. Levinsen, R. S. Christensen, G. M. Bruun and J. J. Arlt, 'Observation of Attractive and Repulsive Polarons in a Bose-Einstein Condensate', Phys. Rev. Lett. **117**, 055302 (2016).

[33] B. Bylicka, D. Chruscinski and S. Maniscalco, 'Non-Markovianity and reservoir memory of quantum channels: a quantum information theory perspective', Sci. Rep. **4**, 5720 (2014).

[34] J.-B. Yuan, H.-J. Xing, L.-M. Kuang and S. Yi, 'Quantum non-Markovian reservoirs of atomic condensates engineered via dipolar interactions', Phys. Rev. A **95**, 033610 (2017).

[35] W. D. Phillips and H. Metcalf, 'Laser deceleration of an atomic beam', Phys. Rev. Lett. **48**, 596 (1982).

[36] M. Krstajic, 'Erbium BEC in an Optical Box Potential', 1st year PhD report (University of Cambridge, July 2018).

[37] N. B. Vilas, 'Laser Cooling Towards a Dipolar Quantum Gas of Erbium Atoms', MPhil thesis (University of Cambridge, July 2018).

[38] K. Dieckmann, R. J. C. Spreeuw, M. Weidemüller and J. T. M. Walraven, 'Two-dimensional magneto-optical trap as a source of slow atoms', Phys. Rev. A **58**, 3891 (1998).

[39] A. Frisch, 'Dipolar Quantum Gases of Erbium', PhD thesis (Leopold-Franzens-Universität Innsbruck, Oct. 2014).

[40] R. Grimm, M. Weidemüller and Y. B. Ovchinnikov, 'Optical Dipole Traps for Neutral Atoms', in *Adv. At. Mol. Opt. Phys.* Vol. 42, edited by B. Bederson and H. Walther (Academic Press, 2000), pp. 95–170.

[41] M. Greiner, I. Bloch, T. W. Hänsch and T. Esslinger, 'Magnetic transport of trapped cold atoms over a large distance', Phys. Rev. A **63**, 031401 (2001).

[42] J. Goldwin, S. Inouye, M. L. Olsen, B. Newman, B. D. DePaola and D. S. Jin, 'Measurement of the interaction strength in a Bose-Fermi mixture with ^{87}Rb and ^{40}K', Phys. Rev. A **70**, 021601 (2004).

[43] H. J. Lewandowski, D. M. Harber, D. L. Whitaker and E. A. Cornell, 'Simplified System for Creating a Bose–Einstein Condensate', J. Low Temp. Phys. **132**, 309 (2003).

[44] T. L. Gustavson, A. P. Chikkatur, A. E. Leanhardt, A. Görlitz, S. Gupta, D. E. Pritchard and W. Ketterle, 'Transport of Bose-Einstein Condensates with Optical Tweezers', Phys. Rev. Lett. **88**, 020401 (2001).

[45] J. Léonard, M. Lee, A. Morales, T. M. Karg, T. Esslinger and T. Donner, 'Optical transport and manipulation of an ultracold atomic cloud using focus-tunable lenses', New J. Phys. **16**, 093028 (2014).

[46] S. Baier, 'An optical dipole trap for Erbium with tunable geometry', Master's thesis (Leopold-Franzens-Universität Innsbruck, Oct. 2012).

[47] T. Schaich, 'A Tunable Optical Dipole Trap for Erbium', Part III project report (University of Cambridge, May 2018).

[48] M. Lepers, J.-F. Wyart and O. Dulieu, 'Anisotropic optical trapping of ultracold erbium atoms', Phys. Rev. A **89**, 022505 (2014).

[49] C. Kohstall, 'A New Toolbox for Experiments with Ultracold ^{6}Li', Master's thesis (Leopold-Franzens-Universität Innsbruck, Feb. 2007).

[50] P. Juhász, 'Precision transport of atoms in a tuneable optical tweezer', Part III project report (University of Cambridge, May 2018).

[51] A. E. Siegman, *Lasers* (Oxford University Press, Oxford, England, 1986).

[52] Y.-J. Lin, A. R. Perry, R. L. Compton, I. B. Spielman and J. V. Porto, 'Rapid production of ^{87}Rb Bose-Einstein condensates in a combined magnetic and optical potential', Phys. Rev. A **79**, 063631 (2009).

[53] W. Ketterle and N. V. Druten, 'Evaporative Cooling of Trapped Atoms', in *Adv. At. Mol. Opt. Phys.* Vol. 37, edited by B. Bederson and H. Walther (Academic Press, 1996), pp. 181–236.

[54] C. Politi, 'Optical dipole trap for an erbium and dysprosium mixture', Master's thesis (Università di Pisa, June 2017).